

ON-SITE SELF-CALIBRATION USING PLANAR FEATURES FOR TERRESTRIAL LASER SCANNERS

Kwang-Ho Bae and Derek D. Lichti

The Institute for Geoscience Research and Department of Spatial Sciences,
Curtin University of Technology, GPO Box U1987, Perth, WA 6845, Australia,
Cooperative Research Centre for Spatial Information (CRC-SI), Australia
k.h.bae@curtin.edu.au, d.lichti@curtin.edu.au

Commission V, WG 3

KEY WORDS: Calibration, Systematic error, Planar targets, Laser Scanning

ABSTRACT:

Terrestrial laser scanners provide a three-dimensional sampled representation (i.e. point cloud) of the surfaces of objects. They have great potential to improve the measurement and representation of remote and widespread objects for applications such as engineering metrology, cultural heritage recording and forestry, among others. Prior to performing measurement tasks such as these, proper error modelling and estimation is essential in order to remove the inherent systematic effects such as range finder offset, collimation axis error, etc.. A rigorous, point-based self-calibration method has been demonstrated to be effective, but it is very labour-intensive since it requires manual measurement of a large number of signalised targets. In this paper, we propose a planar-feature-based “on-site” self-calibration method that can reduce the manual labour needed in the point-based method. After outlining the principles and mathematical models of the proposed method, the subject of model identification is addressed. Tests with simulated datasets reveal that the residual patterns from the plane-based method are markedly different from those of the point-based method. The ramification of this outcome is that systematic error identification, an important process for new instrumentation such as terrestrial laser scanners, is not straightforward. In addition, the tests of the proposed method with real terrestrial laser scanner datasets are presented and analysed.

1. INTRODUCTION

Terrestrial laser scanners (TLSs) have emerged as new measurement instruments for surveying, photogrammetry and computer vision for their fast data acquisition time to measure a three-dimensional point cloud of objects in a matter of minutes. Consequently, the scientific and practical interest in developing calibration procedures to remove systematic errors inherent in terrestrial laser scanner datasets has expanded.

In photogrammetry, “on-site” or “on-the-job” calibration methods are often used as an alternative to laboratory calibration (Luhmann et al., 2007). This is particularly relevant when the temporal stability of the camera used is in doubt. This procedure is performed by imaging portable frames or targets positioned beside the object(s) of interest. Exterior orientation, object space points and camera calibration parameters are estimated simultaneously. In this paper, we propose an on-site calibration method for terrestrial laser scanners using planar features in the point cloud.

Much work has been done on point-based TLS calibration by exploiting their similarities with theodolites or total stations, (e.g. Lichti and Franke, 2005; Lichti and Licht, 2006; Lichti, 2007; Reshetyuk, 2006). Amiri Parian and Grün (2005) developed a point-based calibration method by based on a panoramic camera model for the Z+F Imager 5003. Gielsdorf et al. (2004), however, proposed error models and a calibration method using planar targets for their own low-cost laser scanner.

Though the point-based methods are rigorous and have been shown to be effective, their principal drawback is the need to

manually measure a large number of targets. The use of planar features is therefore favoured as their extraction from point clouds can be highly automated, though it is recognised that signalised target extraction and measurement could also be automated to a large extent. An on-site calibration method has been pursued due to the apparent instability of the calibration parameters (as reported in Lichti, 2007) of the instrument under investigation, the FARO 880 laser scanner. The idea is that calibration can be performed on-site using planar features that exist on many industrial and heritage recording sites, for example, with minimal manual labour.

After outlining the principles and mathematical models of the proposed method, the subject of model identification is addressed. Tests with simulated datasets are undertaken to explore the difference in the residual patterns from the plane-based and point-based methods. In addition, the precision of the proposed method with terrestrial laser scanner datasets is presented and analysed.

2. PLANE-BASED CALIBRATION

2.1 Observation equation

The spherical co-ordinate observations of the i^{th} object space point in the j^{th} scanner space are range, ρ_{ij} , horizontal direction, θ_{ij} , and elevation (vertical) angle, α_{ij} , which are parameterised in terms of scanner space Cartesian co-ordinates (x_{ij}, y_{ij}, z_{ij}) as follows:

$$\rho_{ij} = \sqrt{x_{ij}^2 + y_{ij}^2 + z_{ij}^2} + \Delta p \quad (1)$$

$$\theta_{ij} = \arctan\left(\frac{y_{ij}}{x_{ij}}\right) + \Delta\theta \quad (2)$$

$$\alpha_{ij} = \arctan\left(\frac{z_{ij}}{\sqrt{x_{ij}^2 + y_{ij}^2}}\right) + \Delta\alpha \quad (3)$$

The spherical observation correction terms are given by Lichti (2007) as follows:

$$\begin{aligned} \Delta\rho = & A_0 + A_2 \sin(\alpha_{ij}) + A_3 \sin\left(\frac{4\pi}{U_1} \rho_{ij}\right) \\ & + A_4 \cos\left(\frac{4\pi}{U_1} \rho_{ij}\right) + A_5 \sin\left(\frac{4\pi}{U_2} \rho_{ij}\right) \\ & + A_6 \cos\left(\frac{4\pi}{U_2} \rho_{ij}\right) + A_7 \sin(4\theta_{ij}) + A_8 \cos(4\theta_{ij}) \end{aligned} \quad (4)$$

$$\begin{aligned} \Delta\theta = & B_1 \sec(\alpha_{ij}) + B_2 \tan(\alpha_{ij}) + B_3 \sin(2\theta_{ij}) \\ & + B_4 \cos(2\theta_{ij}) + B_5 \theta_{ij} + B_6 \cos(3\alpha_{ij}) + B_7 \cos(4\alpha_{ij}) \end{aligned} \quad (5)$$

$$\Delta\alpha = C_0 + C_2 \sin(\alpha_{ij}) + C_3 \sin(3\theta_{ij}) + C_4 \cos(3\theta_{ij}) \quad (6)$$

where the sensor-driven additional parameters (APs) for terrestrial laser scanners for range, horizontal direction and elevation angle components of the observations are expressed as A, B and C, respectively. The term U_1 in Eq. 4 represents half the finest modulating wavelength, which is approximately equal to 0.6m. The term U_2 in Eq. 4 equals one-half the median unit length, which is approximately 4.8m. These terms need to be included since the FARO 880 scanner measures range on the basis of the phase-difference method. The aim of a plane-based calibration procedure is to accurately estimate these proposed additional parameters with low correlation among the exterior orientation and plane parameters and other APs.

The problem underlying terrestrial laser scanner calibration is that of model identification. Some systematic error sources, such as those common to total stations, are expected to be observed in the residuals from a registration-only least-squares adjustment. Investigation of these residual patterns has permitted us to develop a systematic error model for laser scanners.

The models can be categorised to two groups: the physical and empirical additional parameters. The physical interpretation of latter is not necessarily apparent, although their systematic trends may be observed in the residuals of a highly redundant and geometrically strong, minimally constrained least-squares adjustment. Detailed description of all the additional parameters and their residual plots can be found in Lichti and Licht (2006), Lichti and Franke (2005) and Lichti (2007).

2.2 Formulation of the proposed plane-based calibration

The proposed plane-based self-calibration method utilises the combined least-squares method that minimises the distance between points and their corresponding planes with a constraint condition. The exterior orientation, plane and the additional

parameters presented in Eqs. 4-6 can be simultaneously estimated. Since the observations and parameters of the point-on-plane condition equation are not separable and each condition includes more than one observation, the combined (or Gauss-Helmert) adjustment model is used.

Let $\mathbf{x} \in \mathbb{R}^u$ be the parameter vector and $\mathbf{l} \in \mathbb{R}^n$ be the observation vector, where u and n are the number of parameters and observations, respectively. Let $f_{ijk}(\mathbf{x}, \mathbf{l})$ be the distance function between the i^{th} point in the j^{th} scanner space (\mathbf{p}_{ij}) and the k^{th} plane target in the object space whose normal vector and orthogonal distance from the origin are $\mathbf{n}_k = (a_k, b_k, c_k)$ and d_k , respectively. The distance function is given as

$$f_{ijk}(\mathbf{x}, \mathbf{l}) = \mathbf{n}_k^T (\mathbf{M}_j^T \mathbf{p}_{ij} + \mathbf{Tr}_j) - d_k = 0 \quad (7)$$

where \mathbf{M}_j and \mathbf{Tr}_j are the rotation and translation parameters between the object and j^{th} scanner spaces, respectively. In other words, this is the condition function for the registration between multiple point clouds and one fixed scan, i.e. the object space. Then the linearised equation for the Gauss-Helmert model is given by

$$\mathbf{A} d\mathbf{x} + \mathbf{B} \mathbf{v} + \mathbf{w}_0 = 0 \quad (8)$$

where m is the total number of point observations, $\mathbf{A} \in \mathbb{R}^{m \times u}$ and $\mathbf{B} \in \mathbb{R}^{m \times n}$ are the Jacobians of $f_{ijk}(\mathbf{x}, \mathbf{l})$ with respect to \mathbf{x} and \mathbf{l} , respectively, \mathbf{v} is the residual vector, \mathbf{w}_0 is the misclosure vector and $d\mathbf{x}$ is the vector of corrections to the approximate parameter values. In its current form, the adjustment is minimally constrained since the inner constraint equations for plane parameters are still under development.

Note that u equals the sum of u_e , u_{ap} and u_p where u_e is the number of the transformation parameters, u_{ap} is the number of the additional parameters and u_p is the number of plane parameters, respectively. The unit length constraint on the direction cosines for each plane is given as

$$g_k(a_k, b_k, c_k, d_k) = \mathbf{n}_k^T \mathbf{n}_k - 1 = 0 \quad (9)$$

and the linearised constraint equation can be given as

$$\mathbf{A}_c d\mathbf{p} + \mathbf{w}_c = \mathbf{v}_c \quad (10)$$

where $\mathbf{A}_c \in \mathbb{R}^{c \times up}$ is the Jacobian of $g_k(a_k, b_k, c_k, d_k)$ with respect to the k^{th} plane target, $d\mathbf{p}$ is the vector of corrections to the approximate plane parameter values and c is the number of constraints. The cost function to be minimised with respect to

$$\begin{aligned} \varphi = & \mathbf{v}^T \mathbf{P} \mathbf{v} + \mathbf{v}_c^T \mathbf{P}_c \mathbf{v}_c + 2\mathbf{k}^T (\mathbf{A} d\mathbf{x} + \mathbf{B} \mathbf{v} + \mathbf{w}_0) \\ & + 2\mathbf{k}_c^T (\mathbf{A}_c d\mathbf{p} + \mathbf{w}_c - \mathbf{v}_c) \end{aligned} \quad (11)$$

where \mathbf{P} and \mathbf{P}_c are the weight matrices for point observations and the constraint for the plane parameters, respectively, and \mathbf{k} and \mathbf{k}_c are the Lagrange multiplier vectors. Minimisation of the cost function leads to the following system of normal equations

$$\mathbf{N} d\mathbf{x} + \mathbf{w} = 0 \quad (12)$$

where

$$\mathbf{N} = \mathbf{A}^T (\mathbf{B} \mathbf{P}^{-1} \mathbf{B}^T)^{-1} \mathbf{A} + \begin{bmatrix} \mathbf{0} & \mathbf{0} \\ \mathbf{0} & \mathbf{A}_c^T \mathbf{P}_c \mathbf{A}_c \end{bmatrix} \quad (13)$$

and

$$\mathbf{w} = \mathbf{A}^T (\mathbf{B} \mathbf{P}^{-1} \mathbf{B}^T)^{-1} \mathbf{w}_0 + \begin{bmatrix} \mathbf{0} \\ \mathbf{A}_c^T \mathbf{P}_c \mathbf{w}_c \end{bmatrix}. \quad (14)$$

2.3 Nonlinear least-squares

The Newton-Raphson solution method can be successfully utilised for point-based calibration (Amiri Parian and Grün, 2005; Lichti, 2007). In the case of plane-based calibration, the inclusion of the point-on-plane condition equations renders the cost function highly nonlinear and thus a nonlinear least-squares method is required in order for the solution to converge rapidly to a global minimum (Shewchuk, 1994; Golub and Van Loan, 1989; Teunissen, 1990).

The normal equations for the proposed method with the Gauss-Helmert model from Eq. 12 can be expressed as

$$\frac{\partial^2 \varphi}{\partial \mathbf{x}^2} d\mathbf{x} + \frac{\partial \varphi}{\partial \mathbf{x}} = \mathbf{0}. \quad (15)$$

When the cost function is either linear or can be linearised, the solution of Eq. 15 is given by

$$d\mathbf{x} = - \left(\frac{\partial^2 \varphi}{\partial \mathbf{x}^2} \right)^{-1} \frac{\partial \varphi}{\partial \mathbf{x}}, \quad (16)$$

which is a special case of the gradient-descent method (Shewchuk, 1994). In the case of the minimisation of nonlinear cost functions, the gradient of the cost function given in Eq. 10 may not be the optimal direction for searching the solution. Therefore, the conjugate gradient method proposes to search a solution in a direction calculated from $-\frac{\partial \varphi}{\partial \mathbf{x}}$ using Gram-Schmidt orthogonalisation (Shewchuk, 1994). Details of the conjugate gradient method and its implementation can be found in Shewchuk (1994) and Golub and Van Loan (1989).

2.4 Outlier detection

The reliability matrix, standardised residuals and variance component estimation (Baarda, 1968; Schaffrin, 1997; Cothren, 2005) are utilised for outlier detection in the proposed plane-based calibration method. For the linearised Gauss-Helmert model equations given (Eq. 12), the reliability matrix \mathbf{R} is given by

$$\mathbf{R} = \mathbf{P}^{-1} \mathbf{B}^T \bar{\mathbf{P}}^{-1} (\mathbf{I}_n - \mathbf{A} \mathbf{N}^{-1} \mathbf{A} \bar{\mathbf{P}}^{-1}) \mathbf{B} \quad (17)$$

where \mathbf{P} is the weight matrix, $\bar{\mathbf{P}} = \mathbf{B} \mathbf{P}^{-1} \mathbf{B}^T$, and \mathbf{I}_n is the identity matrix with rank of n . The i^{th} standardised residual r_i is calculated from its corresponding a priori observation precision, σ_i , the i^{th} component of the residual vector, v_i , and i^{th} diagonal element of \mathbf{R} , R_{ii} , as

$$r_i = \frac{v_i}{\sigma_i \sqrt{R_{ii}}}. \quad (18)$$

Assuming that a priori variance factor is known is conducted under the standard null hypothesis that the standardised residual follows a zero-mean, unit variance Gaussian density function (Schaffrin, 1997; Cothren 2005).

3. EXPERIMENTS

The subject of the self-calibration experiments described herein is the FARO 880 TLS. Two sets of experiments are described in the following sub-sections. The first used simulated data in order to learn how the various systematic errors manifest themselves in the residuals and to investigate the accuracy of AP estimation. The second use real data in which the results are compared to those from point-based calibration.

3.1 Model identification using residual patterns

Eight simulated point clouds of a room (dimensions 4.0m x 10m x 10m) were generated from two different scanner locations (4 orthogonal scans were captured at each position). The distance between two scanners was 8m and the height of the scanner was set to 2m. Six 1.5m x 1.5m planar targets on were simulated to lie in the centre of each wall, the floor and the ceiling of the room. The sampling was such that each target had 100 points—see Figure 3a. In short, the simulated dataset represents the point clouds captured by an ideal laser scanner in a test room with perfectly flat walls, floor and ceiling.

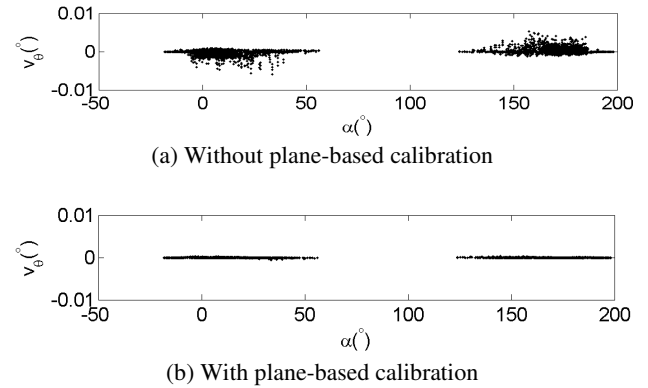


Figure 1. Residuals of the plane-based calibration method in the presence of a collimation axis error ($B1=50''$) for the simulated dataset.

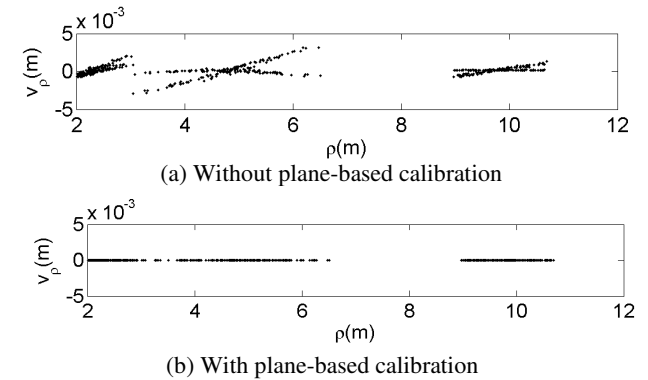


Figure 2. Residuals of the plane-based calibration method in the presence of a rangefinder additive constant ($A_0=1\text{mm}$) for the simulated dataset

The systematic errors of terrestrial laser scanners described in Eqs. 4-6 were first added one-by-one to the error-less, simulated point clouds. In a point-based method, most misclosure patterns appear very similar to functional form of the corresponding systematic error model (Lichti, 2007). For example, the vertical eccentricity error, C_2 in Eq. 6, can be observed as a sine function of the elevation angle in the residual pattern of the point-based method.

Figures 1 and 2 are plots of residual due to collimation axis error (B_1) and rangefinder additive constant (A_0), respectively. These residual patterns are quite different from those observed in the point-based calibration method (Lichti and Franke, 2005) in which the residuals appear as the expected secant function for collimation axis error and the effect of the rangefinder offset is manifest as a linear function of range due to correlation with the positional elements of exterior orientation. These differences make it difficult to identify the systematic errors in the residuals from plane-based self-calibration.

3.2 Optimal locations of laser scanners with simulated data

An empirical investigation into optimal laser scanner location for the plane-based self-calibration was also conducted under the previously-described conditions. This investigation with simulated datasets in Figure 3 was based on the ratio of the estimated additional parameter to the true value, i.e. artificially added systematic error to the simulated data. With one of the two scan locations fixed at location “101” shown in Figure 3b, point clouds for the second position were simulated from each of the 9 locations “102” to “110”. We found that the accuracy of the range and elevation angle additional parameters was as high as 99% for this test. On the other hand, the accuracy of the collimation axis error (B_1) varies in different laser scanner combinations.

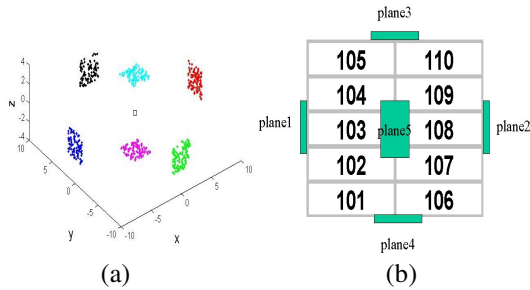


Figure 3. (a) Simulated point clouds for finding the optimal scanner locations. Square sign is the centre of the test room. (b) The scanner is located in the centre of each cell, e.g. 105. The height of the scanner is 2m.

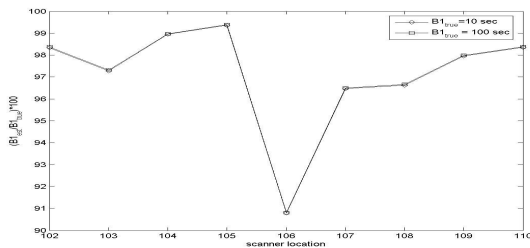


Figure 4. The ratio between the estimated and true B_1 for different laser scanner locations when the first location of the scanner is 101 in Figure 3(b).

For all combinations of scanner locations in Figure 3(b), the accuracy of the estimated APs was high except for the collimation axis error, B_1 . The ratio of its estimated to true value was found to be strongly dependent on the scanner location, as can be seen in Figure 4. This additional parameter is accurately estimated at all locations except for the combination of 101 and 106. For the collimation axis error, the best laser scanner combinations were 105 and 110 with the location 101 in the case of this test room.

3.3 Accuracy tests with simulated datasets

The plane-based self-calibration method was applied to the simulated data described in the previous section. Two systematic errors, A_0 and B_1 , were added to the error-less point clouds. The standard deviations of residuals for the range, horizontal direction and elevation angle without correction, with correction of A_0 only and with correction of A_0 and B_1 are given in Table 1. In addition, the residual patterns of these cases are presented in Figure 5. Clear improvements in all spherical observations were observed and, in particular, that of elevation angle is the largest. The difference between the standard deviations of range in the cases with A_0 correction only and with A_0 and B_1 correction is on the order of 10. This suggests that a priori knowledge of the existing systematic error, i.e. A_0 and B_1 , is required in order to achieve the maximum observational precision from calibration since, as already mentioned and can be seen in Figure 5a, model identification is difficult.

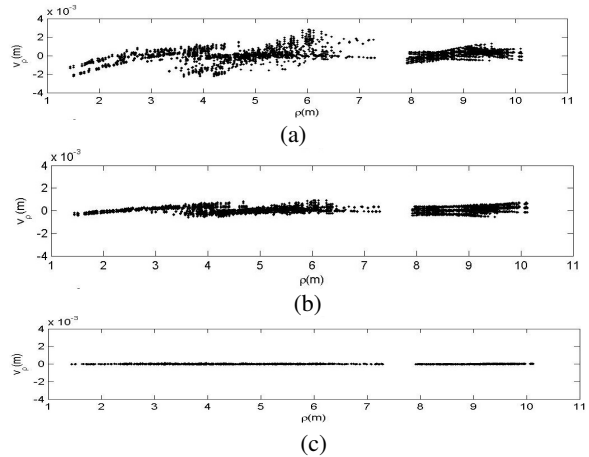


Figure 5. Residual plots in the presence of rangefinder additive constant (A_0) and the collimation axis error (B_1). (a) Without calibration (i.e. registration only) (b) with A_0 only (c) with A_0 and B_1

	No correction	A_0	A_0 and B_1
STD v_ρ (mm)	0.70	0.24	0.02
STD v_θ (")	1.00	0.42	0.03
STD v_α (")	1.50	0.03	0.04

Table 1. Residual statistics of the plane-based self-calibration method in three different cases: without correction (registration only), with A_0 correction only, and with A_0 and B_1 correction. STD is the standard deviation.

A further series of accuracy tests was conducted in which a range of possible AP values was added to the simulated dataset. The range for rangefinder additive constant (A_0) was 0.25mm to

10mm, 10" to 200" for the collimation axis error (B_1) and for the vertical circle index error (C_0) was 10" to 100". These values were chosen for consistency with other studies (e.g. Lichti and Licht, 2006). A maximum bias of 0.006% was observed for all three additional parameters, with larger values generally being estimated more accurately. Some difficulty in the estimation of collimation axis error is expected when the magnitude of the applied B_1 is increased as shown in Figure 5(b). For example, from Table 1, we observed a slight increase in v_α in

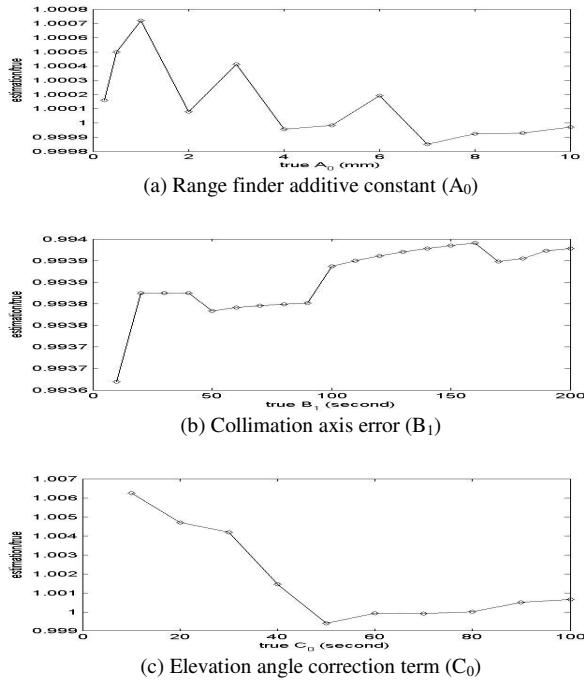


Figure 6. Accuracy of some additional parameters with simulated datasets, which defined as the ratio of the true and estimated parameters.

3.4 Estimation of the APs of the FARO 880 from real data

The FARO 880 terrestrial laser scanner offers a near spherical field of view made possible by a 320° vertical angle scanning range and a 180° horizontal field of view. The scanner features two orthogonal inclinometers that correct the captured data for instrument tilt. The manufacturer specifies 0.01° ($36''$) for the inclinometer accuracy and 3mm linearity error at 10m with 84% target reflectivity for the rangefinder. See Lichti (2007) for a description of its salient properties.

Two datasets, named here Data1 (28 October/2005) and Data2 (7 December/2005), captured with the FARO 880, were utilised for the test. A total of eight point clouds of a room were captured from two locations. The scanner was manually rotated on the tripod by 90° after each of the set of four scans was captured.

The dimension of the room in Data1 is (H, W, L) = (3m, 5m, 9m) with 18 planar targets. The nominal distance between the two scanner locations was 4m. The radial distance from the laser scanner to the object was approximately from 1.5m to 7.5m. The plane-based calibration adjustment (minimally constrained) had 5641 observations with 5538 degree of freedom. The dimension of the room Data2 is (H, W, L) = (3m, 9m, 12m) with 25 planar targets. The nominal distance between

the two scanner locations was 6.7m. The radial distance from the laser scanner to the object was approximately from 2m to 10m. The plane-based calibration adjustment (minimally constrained) had 8231 observations with 8107 degree of freedom.

Note that the planar targets for this on-site calibration were manually extracted from wall, ceiling and floors of the original point clouds and some obvious outliers were removed by investing the results of the first order plane fit. For the proposed plane calibration method, spherical coordinate observations were derived from the Cartesian coordinates exported using the commercial software, iQscene. Variance component estimation and the outlier detection method explained in Section 2.5 were used to optimise the contribution of each of the three groups of spherical observables.

For the point-based calibration with the room Data1, 134 planar, A4-size targets were mounted on all four walls, the floor and the ceiling. Target center measurement was conducted using the commercial software, iQscene. The point-based calibration method (with free-network) adjustment had 2469 observations with 2019 degrees of freedom. For the point-based calibration with the room Data2, 131 planar, A4-size targets were mounted on all four walls, the floor and the ceiling. The point-based calibration method (with free-network) adjustment had 2193 observations with 1738 degrees of freedom.

	Without self-calibration	With calibration	Improvement (%)
STD v_p (mm)	1.2	1.2	5.4
STD v_θ (")	67.9	18.6	72.6
STD v_α (")	24.3	19.9	18.4

Table 2. Residual statistics from plane-based calibration after outlier removal for Data1 (28 October/2005).

	Without self-calibration	With calibration	Improvement (%)
STD v_p (mm)	2.4	1.9	21.0
STD v_θ (")	86.3	35.2	59.2
STD v_α (")	51.8	46.5	10.3

Table 3. Residual statistics from point-based calibration after outlier removal for Data1 (28 October/2005).

	Without self-calibration	With calibration	Improvement (%)
STD v_p (mm)	1.0	0.8	21.4
STD v_θ (")	49.2	47.3	3.8
STD v_α (")	55.3	49.5	10.6

Table 4. Residual statistics from plane-based calibration after outlier removal for Data2 (7 December/2005).

	Without self-calibration	With calibration	Improvement (%)
STD v_p (mm)	2.3	1.7	26.1
STD v_θ (")	109.8	36.7	66.6
STD v_α (")	65.88	20.9	68.3

Table 5. Residual statistics from point-based calibration after outlier removal for Data2 (7 December/2005).

Only a reduced set of the additional parameters (A_0 , B_1 , B_2 , B_3 , B_4 , C_0 and C_2) was used for all calibrations. The standard

deviations of the residuals for the range, horizontal and elevation angle for both the plane- and point-based methods are given in Tables 2 and 4. Both datasets showed significant improvement in the precision of all spherical observations.

The plane-based calibration provided greater precision in the spherical observables than did the point-based method. In contrast, Lichti and Licht (2006) reported a similar level of point observational precision with all physical and empirical additional parameters of terrestrial laser scanners.

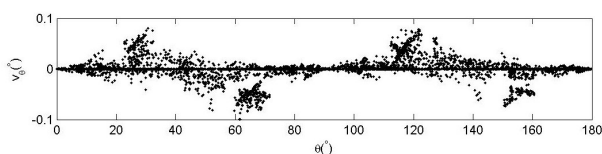


Figure 7. Horizontal direction residual vs horizontal direction without plane-based self-calibration (Data1).

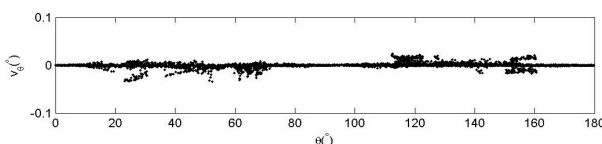


Figure 8. Horizontal direction residual vs horizontal direction with plane-based calibration (Data1).

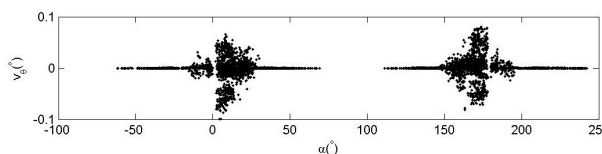


Figure 9. Horizontal angle residuals vs elevation angle without plane-based self-calibration (Data1).

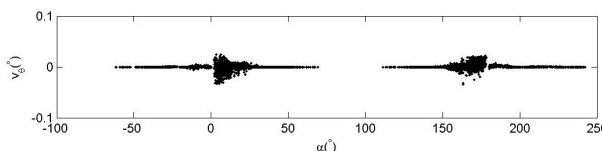


Figure 10. Horizontal angle residual vs elevation angle with plane-based self-calibration (Data1).

Plots of the residuals of horizontal direction angle both with and without, additional parameter correction from the plane-based case are presented in Figures 7-10. Although they clearly show an improvement in the precision of the observations, they also show residual systematic effects that are likely due to unmodelled errors since only a reduced-AP model has been implemented thus far.

4. CONCLUSIONS

A plane-based self-calibration method based on terrestrial laser scanner systematic error modelling has been presented and has been demonstrated to improve observational precision of the self-calibration residual standard deviation up to 72.6% with the help of outlier detection and variance component estimation.

The contributions of this paper can be summarised as follows: First, the residual patterns of the plane-based calibration method are shown to be different from the functional models of systematic errors. This could cause great difficulty in systematic

error model identification, not only for formulating error models but also for confirmation of the removal of the targeted systematic errors. Second, the results of the plane-based calibration are improved over those of the point-based method, although there are some difficulties in the accurate estimation of some known additional parameters.

5. ACKNOWLEDGEMENTS

This work has been supported by Curtin University of Technology and the Cooperative Research Centre for Spatial Information, whose activities are funded by the Australian Commonwealth's Cooperative Research Centres Programme.

REFERENCES

- Amiri Parian, J. and A. Grün, 2005. Integrated laser scanner and intensity image calibration and accuracy assessment. In: *The International Archives of the Photogrammetry, Remote Sensing and Spatial Information Sciences*, Vol. 36 (Part 3/W19), pp. 18-23.
- Baarda, W., 1968. A testing procedure for use in geodetic networks. In: *Publication on Geodesy*, Netherlands Geodetic Com., Delft, The Netherlands, 2(5)
- Cothren J., 2005. Reliability in constrained Gauss-Markov models: an analytical and differential approach with applications in Photogrammetry, In: Ph.D. dissertation, Department of Civil and Environmental Engineering and Geodetic Science, Ohio State University, Columbus, USA, 61 pages
- Gielsdorf, F., A. Rietdorf and L. Gruendig, 2004. A Concept for the calibration of terrestrial laser scanners. In: *Proceedings of the FIG Working Week*, Athens, Greece. [On CD-ROM].
- Golub G. H. and Van Loan C. F., 1989. *Matrix computations* (2nd ed.), Johns Hopkins University Press.
- Lichti, D.D. and J. Franke, 2005. Self-calibration of the iQsun 880 laser scanner. In: *Optical 3-D Measurement Techniques VII*, Vienna, Austria, Vol. I, pp. 112-121.
- Lichti, D.D. and M. G. Licht, 2006. Experience with terrestrial laser scanner modelling and accuracy assessment. In: *The International Archives of the Photogrammetry, Remote Sensing and Spatial Information Sciences*, Vol. 36 (Part 5), pp. 155-160.
- Lichti D. D., 2007. Error modelling, calibration and analysis of an AM-CW terrestrial laser scanner system, In: *ISPRS Journal of Photogrammetry and Remote Sensing*, 61 (5), pp. 307-324.
- Luhmann T., S. Robson, S. Kyle and I. Harley, 2007. *Close Range Photogrammetry*, Whittles Publishing
- Reshetyuk, Y., 2006. Calibration of terrestrial laser scanners Callidus 1.1, Leica HDS 3000 and Leica HDS 2500. In: *Survey Review* 38 (302), 703-713.
- Schaffrin B. 1997, Reliability measures for correlated observations. *Journal of Surveying Engineering*, 124 (3), pp. 126-133
- Shewchuk J. R., 1994. An Introduction to the Conjugate Gradient Method Without the Agonizing Pain, In: *Technical Report: CS-94-125*, Carnegie Mellon University, Pittsburgh, PA, USA, 64 pp.
- Teunissen P. J. G., 1990. Nonlinear least squares, In: *Manuscripta Geodaetica*, Vol. 15, pp. 137-150
- von Hansen, W., Michaelsen, E. and Thonnessen, U., 2006. Cluster analysis and priority sorting in huge point clouds for building reconstruction. In: *Proceedings of the 18th International Conference on Pattern Recognition (ICPR'06)*, pp. 23-26.